

Article

Differential Analysis of the Positron Impact Ionization of Hydrogen in Debye Plasmas

Emiliano Acebal ^{*}, Sergio Hernan Martínez and Sebastian Otranto 

Instituto de Física del Sur (IFISUR), Departamento de Física, Universidad Nacional del Sur (UNS), CONICET, Av. L. N. Alem 1253, Bahía Blanca B8000CPB, Argentina

* Correspondence: emiliano.acebal@uns.edu.ar

Abstract: In this work, a theoretical differential analysis of the positron impact ionization of hydrogen embedded in weakly coupled plasmas at an impact energy of 80 eV is developed. While the total and singly differential cross sections are analyzed within the classical trajectory Monte Carlo method, a Born-3DW model for screened environments, recently introduced by the authors, is used to provide a fully differential view of the process. The present results suggest that the electron emission spectra are strongly affected by the level of screening of the surrounding medium, mainly due to the loss of the postcollisional interaction mechanism.

Keywords: ionization; positron impact; Debye plasmas; classical trajectory Monte Carlo; Born-3DW

1. Introduction

During the last seven decades, the study of charged particle collisions with atoms and molecules has represented a challenging research field. Despite the intrinsic interest from a basic science perspective, the roles that these mechanisms play in many areas, such as astrophysics, radiotherapy, and fusion plasmas, have only recently been established and have pushed the focus of research towards a more refined understanding of the physical mechanisms involved.

The dynamics of electron emission processes can be studied at different levels of differentiability. The technological advances between 1950 and 2003 paved the way to move from total cross sections, the least detailed observations in terms of physical mechanisms, to the fully differential cross sections that provide a complete picture of the electron emission process, since the momenta of all the fragments are resolved [1,2]. A constructive interaction between the experimental and theoretical groups in this period led to the simultaneous development of highly accurate detectors and coincidence techniques and sophisticated theoretical treatments, which currently largely rely on heavy computational resources.

Although complete theoretical descriptions, both quantum and semiclassical, have been available for nearly four decades, experimental differential cross sections for atomic ionization by positron impact have only become feasible in recent years [3–7]. These complex experiments provide striking information about ionization processes, which sometimes disagree with the theoretical model under consideration [8,9].

While these advances pertain to the field of collisions with gas phase targets in such low densities that the target atom/molecule can be considered isolated from its surroundings, laboratory and astrophysical environments provide a completely different scenario. The screened interactions modify the electronic structure of the atoms and molecules and also affect the transient dynamics among the colliding particles compared to the unscreened case.

Over the past 15 years, several studies have been devoted to analysing positron collision processes in the plasma environment. A decreasing behavior of the excitation cross section for increasing screening was found by Zhang et al. and the group of Ghoshal [10–13].



Citation: Acebal, E.; Martínez, S.H.; Otranto, S. Differential Analysis of the Positron Impact Ionization of Hydrogen in Debye Plasmas. *Atoms* **2023**, *11*, 15. <https://doi.org/10.3390/atoms11020015>

Academic Editor: Károly Tökési

Received: 14 December 2022

Revised: 2 January 2023

Accepted: 13 January 2023

Published: 18 January 2023



Copyright: © 2023 by the authors. Licensee MDPI, Basel, Switzerland. This article is an open access article distributed under the terms and conditions of the Creative Commons Attribution (CC BY) license (<https://creativecommons.org/licenses/by/4.0/>).

This behavior was in concordance with that obtained from the electron impact studies of Zammit et al. [14,15]. Positronium formation in screened contexts was also studied in the past decade, and the cross sections for the screened case were found to be significantly larger than those corresponding to the unscreened case [16,17].

Aside from the former studies, at present, we are not aware of any reported work, which has analyzed the positron impact ionization of hydrogen embedded in a plasma environment. In this work, we perform a differential analysis of this process at an impact energy of 80 eV. This energy is representative of the region at which the total ionization cross section peaks for the unscreened case and is, therefore, considered statistically relevant. With the aim of providing a more general overview, we complement the classical trajectory Monte Carlo (CTMC) simulations for the Total (TCS) and Singly Differential Cross Sections (SDCS), with Fully Differential Cross Sections (FDSCS) obtained within the screened version of the Born-3DW model [18]. The reason for this combination lies in the fact that in the CTMC model, the computational cost increases as one moves from the TCS to the FDSCS, while in the distorted wave models, the computational cost increases just in the opposite direction. Therefore, the present strategy combines the best of our capabilities at present. In the recently introduced Born-3DW model, the interaction between particles is modeled by means of the Debye–Hückel potential. Fully differential analyses of the electron impact ionization of hydrogen in weakly coupled plasmas exhibited a clear sensitivity in the magnitude and shape of the denominated binary and recoil peaks with the degree of screening. The observed trends have been described in terms of the spatial windows needed for some collisional mechanisms to take place [18].

In Section 2, the theoretical methods employed in this work are briefly described. The results are shown and discussed in Section 3. Finally, conclusions are drawn in Section 4. Atomic units are used throughout this work unless otherwise stated.

2. Materials and Methods

2.1. Classical Trajectory Monte Carlo Method

In this work, the CTMC method in its microcanonical formulation was employed [19–21]. Hamilton’s equations of motion for a mutually interacting three-body system were numerically solved by means of a fourth order Runge–Kutta method with an adaptive step size. The Hamiltonian for this system reads

$$H = \frac{p_1^2}{2m_1} + \frac{p_2^2}{2m_2} + \frac{p_3^2}{2m_3} + V(r_{12}) + V(r_{13}) + V(r_{23}), \quad (1)$$

where the 1, 2, and 3 subscripts stand for the projectile, electron, and nuclear target, respectively. The interaction between particle i and particle j is described by means of the Debye–Hückel model potential,

$$V(r_{ij}) = \frac{Z_i Z_j}{r_{ij}} e^{-\frac{r_{ij}}{r_D}}. \quad (2)$$

Here, the parameter r_D , commonly known as the Debye screening length, is defined as the ratio between the thermal velocity and the plasma frequency $r_D = v_T/\omega_p = \sqrt{k_B T_e / (4\pi e^2 n_e)}$, where k_B is the Boltzmann constant, e is the electron charge, and n_e and T_e are the plasma–electron density and temperature, respectively. It can be seen that lower values of r_D imply higher levels of screening in the environment.

2.2. Born-3DW Model

In the present Born initial state treatment, the transition amplitude for the ionization process can be written as

$$T_{fi} = \langle \Psi_f^- | V_I | \psi_i \rangle. \quad (3)$$

The wave function ψ_i represents the initial state described as the product between the screened hydrogen atom ground state wave function ϕ_i and an incoming projectile plane wave:

$$\psi_i = \frac{1}{(2\pi)^{3/2}} e^{i\mathbf{k}_0 \cdot \mathbf{r}_1} \phi_i(\mathbf{r}_2). \tag{4}$$

Here, \mathbf{r}_1 and \mathbf{r}_2 are the positron and target electron coordinates, respectively, with respect to the nucleus, and \mathbf{k}_0 is the impinging projectile momentum. We have employed Salvat’s code [22] to obtain the ground state wavefunctions ϕ_i for the different r_D -values considered.

The interaction potential V_I is given by the nonresolved part of the Hamiltonian by the initial state ψ_i :

$$V_I(\mathbf{r}_1, \mathbf{r}_2) = \frac{Z}{r_1} e^{-\frac{r_1}{r_D}} - \frac{1}{r_{12}} e^{-\frac{r_{12}}{r_D}}, \tag{5}$$

where $\mathbf{r}_{12} = \mathbf{r}_1 - \mathbf{r}_2$, and Z is the charge of the nucleus.

Finally, the final state wavefunction Ψ_f^- is written as

$$\Psi_f^- = \chi^-(\mathbf{k}_1, \mathbf{r}_1) \chi^-(\mathbf{k}_2, \mathbf{r}_2) \zeta^-(\mathbf{k}_{12}, \mathbf{r}_{12}), \tag{6}$$

with $\mathbf{k}_{12} = (\mathbf{k}_1 - \mathbf{k}_2)/2$, and \mathbf{k}_1 and \mathbf{k}_2 are the final positron and electron momenta, respectively. The wave function $\chi^-(\mathbf{k}_i, \mathbf{r}_i)$ with $i = 1, 2$ represents the final-state continuum wave function for the positron ($i = 1$) and electron ($i = 2$) in the field of the nucleus, and it is given by the following partial wave expansion:

$$\chi^-(\mathbf{k}_i, \mathbf{r}_i) = \sum_{l=0}^{\infty} \frac{(2l+1)}{k_i r_i} i^l e^{-i\delta_l} u_l(k_i, r_i) P_l(\hat{\mathbf{k}}_i \cdot \hat{\mathbf{r}}_i). \tag{7}$$

Here, δ_l is the phase shift with respect to the plane wave. The radial wavefunction $u_l(k_i, r_i)$ fulfills the equation

$$\left[-\frac{1}{2} \frac{d^2}{dr_i^2} + \frac{l(l+1)}{2r_i^2} + V(r_i) \right] u_l(k_i, r_i) = \frac{k_i^2}{2} u_l(k_i, r_i) \tag{8}$$

and, together with δ_l , can be obtained through Salvat’s code [22].

On the other hand, the wavefunction $\zeta^-(\mathbf{k}_{12}, \mathbf{r}_{12})$ represents the screened projectile–electron interaction and is given by

$$\zeta^- = \chi^-(\mathbf{k}_{12}, \mathbf{r}_{12}) (2\pi)^{3/2} e^{-i\mathbf{k}_{12} \cdot \mathbf{r}_{12}}. \tag{9}$$

Since the mass of the particles in this case is the same, to obtain $\chi^-(\mathbf{k}_{12}, \mathbf{r}_{12})$, the interaction potential of Equation (2) was multiplied by the reduced mass $\mu_{12} = m_1 m_2 / (m_1 + m_2) = 1/2$ in Salvat’s code. By doing so, we verified that our final wavefunction reduced to the well-known 3C function [23,24] when the screening was removed.

To evaluate the transition amplitude T_{fi} , we performed a six-dimensional integration using the adaptive Vegas Monte Carlo algorithm [25]. The wavepacket approach of Malcherek and Briggs was used to treat the continuum–continuum transition for the projectile [26].

3. Results and Discussion

In the first place, we present in Figure 1 the CTMC total ionization cross section as a function of the Debye length. For the positron impact, it can be seen that for r_D -values below 20 a.u., the cross section increased, and for $r_D = 1$ a.u., its magnitude was 4.51 times greater than that predicted for $r_D = 100$ a.u. This behavior was in concordance with the previous ion impact ionization on hydrogen embedded in weak plasmas [27]. In addition, we present the calculated electron impact results, where we observed the same behavior

as r_D decreased but with a smaller magnitude. Moreover, we benchmarked these results with more elaborate calculations by means of the convergent-close-coupling (CCC) method from Zammit and co-workers [14], where we observed that both methods were in very good agreement.

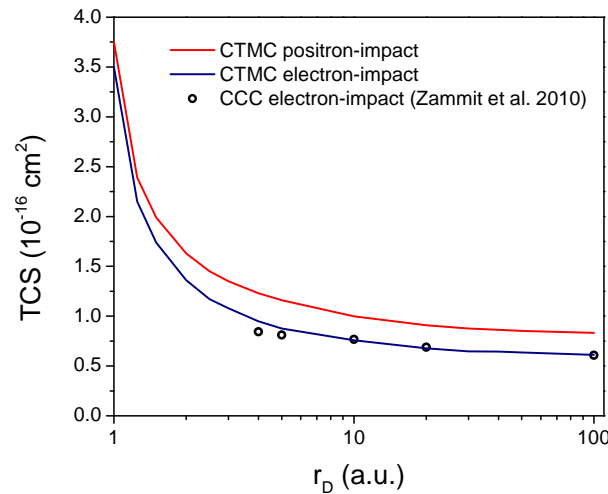


Figure 1. The total ionization cross section as a function of the Debye length r_D . The solid curves are the present CTMC calculations and the open circles are the CCC electron impact calculations from Zammit et al. [14].

Now, moving to the SDCSs, in Figure 2, we show the SDCS as a function of the polar angle of the emitted electron. For large r_D -values, the postcollisional interaction of the emitted electron with the positron focused most of the electronic emission in the forward direction. As the r_D -value was lowered, the structure became less asymmetric. For $r_D = 1$ a.u., a binary peak structure became clearly dominant at about 68° , and no traces of the postcollisional interaction were observed in the forward direction. This was naturally expected due to the following two reasons: on the one hand, this particular r_D value was very close to the minimum screening length needed for a bound state to exist ($r_{D_{min}} = 0.83991$ a.u. [28]); on the other hand, the ionization potential corresponding to $r_D = 1$ a.u. was nearly an order of magnitude lower than for $r_D = 1.5$ a.u. [18].

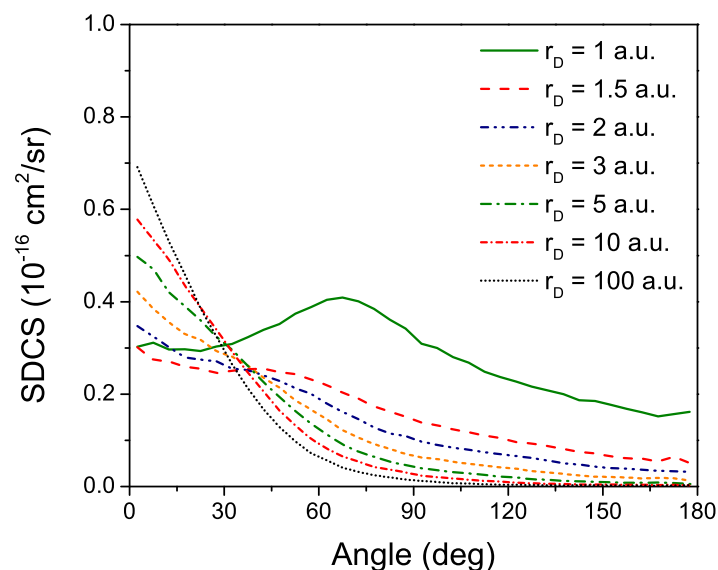


Figure 2. The CTMC singly differential cross section as a function of the electron emission angle for different r_D -values.

In Figure 3, we show the SDCS as a function of the energy of the emitted electron. As a general trend, the emission of low energy electrons was favored, and the intensity of the cross sections increased as the r_D -value was lowered. In contrast to the ion–atom case, where the electrons could attain very large emission energies with a smoothly decreasing probability, for light particle impact, the energy conservation led to a maximum electron energy. This explained the cutoff shown by the SDCS that shifted to larger energies for decreasing r_D -values as a consequence of the decreasing values for the ionization potential [18].

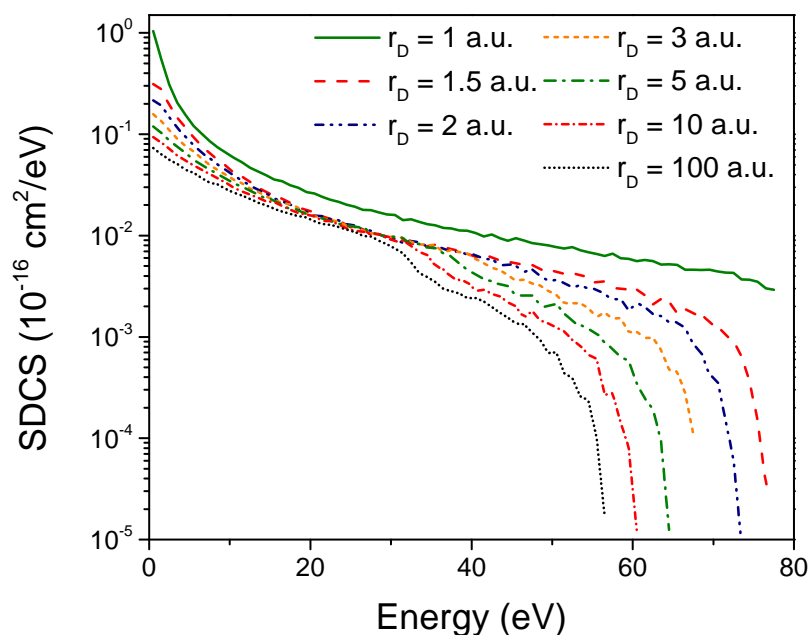


Figure 3. The CTMC singly differential cross section as a function of the emitted electron energy for different r_D -values.

Moving to the fully differential analyses, in Figure 4, we show the FDSCS obtained by means of the Born-3DW model represented in terms of polar plots. The electron emission was restricted to the collision plane defined by the impinging and scattered projectile directions. Electron impact data were also included at this point to highlight the influence of the projectile charge sign. To ease the visualization, the electron data were scaled to the positron data at the maximum of the binary peak. The corresponding factors are explicitly shown in the plots. The FDSCS corresponded to an impact energy of $E_0 = 80$ eV, an electron emitted with an energy $E_2 = 5$ eV, and a projectile scattered by an angle $\theta_1 = -4^\circ$. Debye lengths of 1, 1.5, 2, 3, 5, 10, and 50 a.u. and the unscreened asymptotic limit were explicitly considered. Two main structures are visible: the denominated binary peak, which describes an electron being emitted in the forward direction, and the recoil peak, which describes an electron emitted backwards. The usual physical picture employed to describe these structures is that of an electron first scattered by the projectile with the target nucleus as spectator (binary peak), followed by a secondary collision with the target ion (recoil peak). However, it has been shown already that unless the electron was emitted with a momentum equal to that transferred by the projectile, both binary and recoil peaks imply recoil of the target but in minor or major degrees, respectively [18]. In the present treatment, the Born initial state was identical for the positrons and electrons as projectiles. Therefore, differences arising in the binary peak and recoil structures can be ascribed to the attraction (for positron impact) or repulsion (for electron impact) between the projectile and the emitted electron. Despite the difference in magnitude, the electron and positron impact cases led to clear differences in their structures. As a general trend, i.e. independent of the

r_D -value under consideration, the electron data exhibited a quite noticeable recoil peak structure. For $r_D = 50$ a.u. and the unscreened case, the intensity of the electron-impact recoil peak overcame that of the binary peak. This binary peak was located at angles larger than those corresponding to the momentum transferred by the projectile $\mathbf{q} = \mathbf{k}_0 - \mathbf{k}_1$ due to the postcollisional interaction between the emitted electron and the projectile. As r_D was decreased to 10 a.u. and below, the binary and recoil peaks were comparable in size. The binary peak shifted closer to the momentum transfer direction with respect to the previous cases. As we moved down to $r_D = 1.5$ a.u., we noticed that the binary peak was larger in magnitude and was found closer to the momentum transfer direction. This was a clear indication that the postcollisional interaction effects were lost for large screenings (very low r_D -values). In contrast, the positron data were conformed by a dominant binary peak, and very minor structures were observed for the recoil peak. This behavior was already noticed by Brauner, Briggs, and Klar, in their pioneering positron and electron-impact ionization of hydrogen studies [23] and interpreted in terms of the attraction/repulsion between the emitted electron and the projectile in the final state. As in the electron impact case, the shift in the binary peak with respect to the momentum transfer direction provided clear traces of the postcollisional interaction for large r_D -values. In this case, the shift was toward lower emission angles. Again, these traces were lost as the degree of screening increased. For the lowest r_D value considered (1 a.u.), the FDCS was an order of magnitude lower than that for $r_D = 1.5$ a.u. following the trend observed as the screening was enhanced.

In Figure 5, we show the FDCS corresponding to the same projectile energy and electron emission energy, but the projectile scattering angle was now set at $\theta_1 = -10^\circ$. In this case, for which the momentum transferred by the projectile was larger, we observed for the electron impact that the binary peak became dominant over the recoil peak in the whole r_D -range explored. Again, the recoil peak structure for the electron impact was clearer than the one predicted for the positron impact, and as the r_D decreased, the binary peaks for both projectiles tended to be located in the momentum transfer direction. Moreover, the electron and positron impact binary peaks were in very good agreement.

In Figure 6, we show the FDCS corresponding to the same projectile energy and electron emission energy, but the projectile scattering angle was now set at $\theta_1 = -15^\circ$. This was the largest momentum transferred by the projectile considered in this work. We observed for the electron impact that the dominance of the binary peak over the recoil peak in the whole r_D -range explored was accentuated. Only a very tiny structure provided evidence of a recoil peak in the positron impact case. For $r_D = 1$ a.u., the electron and positron impact FDCS were found to be in very good shape agreement, clearly indicating the absence of a postcollisional interaction.

Finally, in Figure 7, we focused on the case in which both the projectile and the emitted electron, receded in the forward direction ($\theta_1 = \theta_2 = 0^\circ$). This emission geometry was considered particularly relevant, since for positive ions and positrons, a sharp peak was exhibited by the electron spectra at small relative angles and velocity with respect to the projectile. This peak, which is known as the electron capture to the continuum (ECC) peak, was first observed in proton collisions on He by Crooks and Rudd in 1970 [29]. Since then, a large number of studies, both experimental and theoretical, have been developed in order to reproduce the structure in different collisional systems, involving positive ions [30–33] or positrons [3,34,35] as projectiles. The asymmetry of this peak was predicted by quantum mechanical theories that took account of the interaction between the emitted electron with both the target ion and projectile [32,33] and also by CTMC simulations [31]. It is worth noting that electrons must be tracked for long periods of time in the classical treatment to achieve convergence in the structure of the peak.

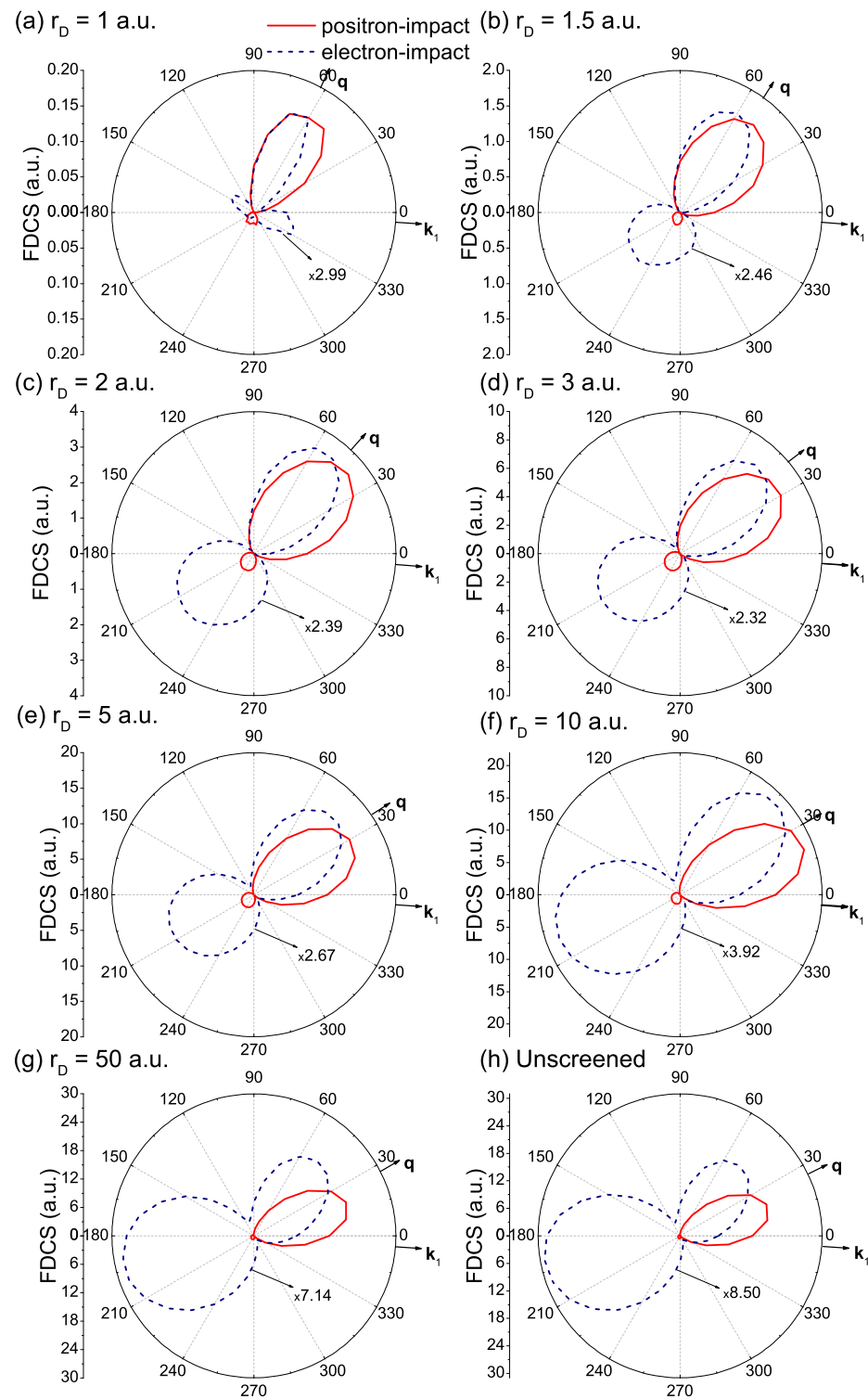


Figure 4. The Born-3DW fully differential cross section in the scattering plane for positron (solid line) and electron (dashed line) impact as a function of the emitted electron angle. The emitted electron energy is 5 eV, and the projectile scattering angle is $\theta_1 = -4^\circ$ (\mathbf{k}_1 indicated in the polar plots). Cross sections are shown for different r_D -values. The unshielded asymptotic limit is also presented.

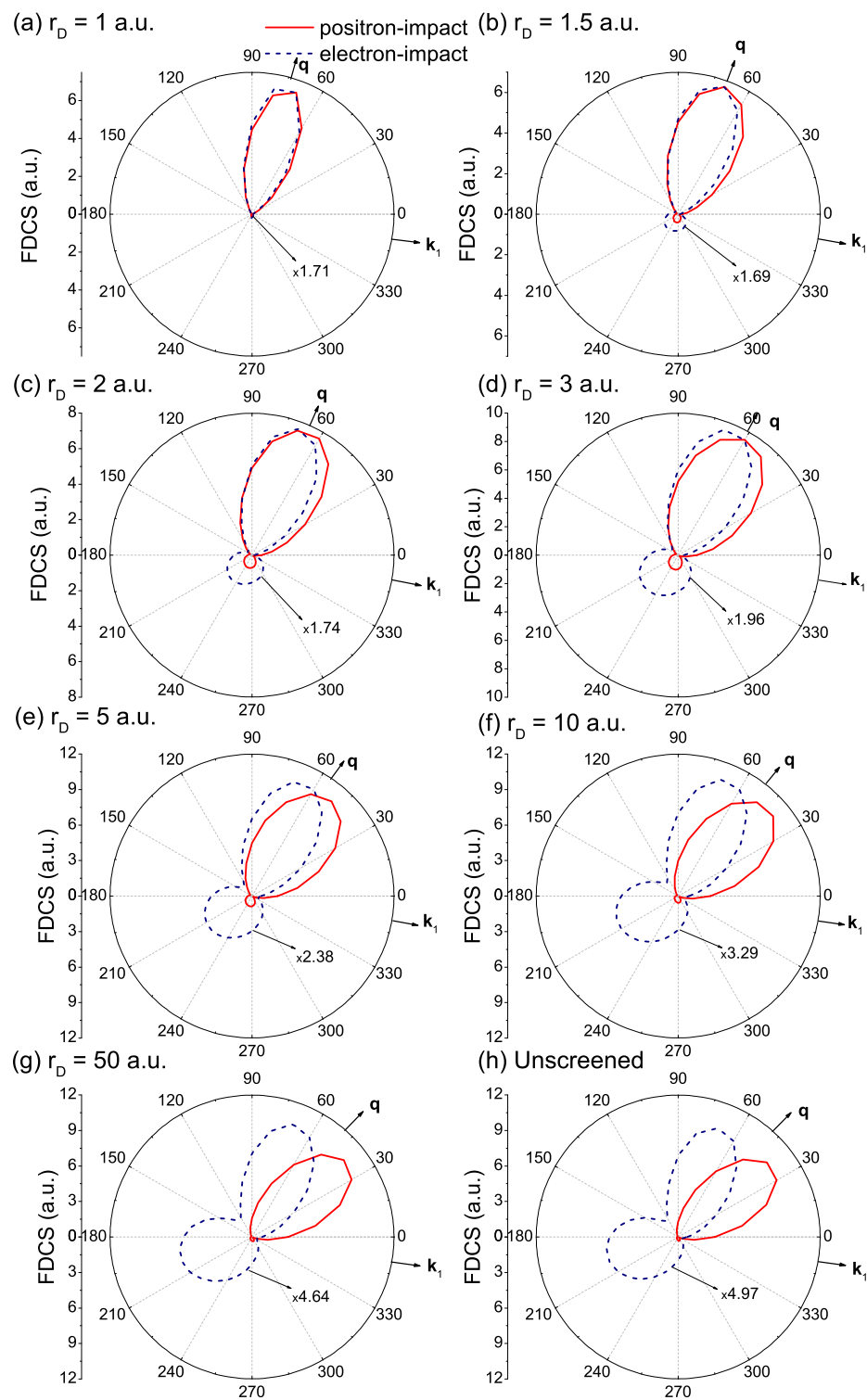


Figure 5. The same visualization as in Figure 4 but for $\theta_1 = -10^\circ$.

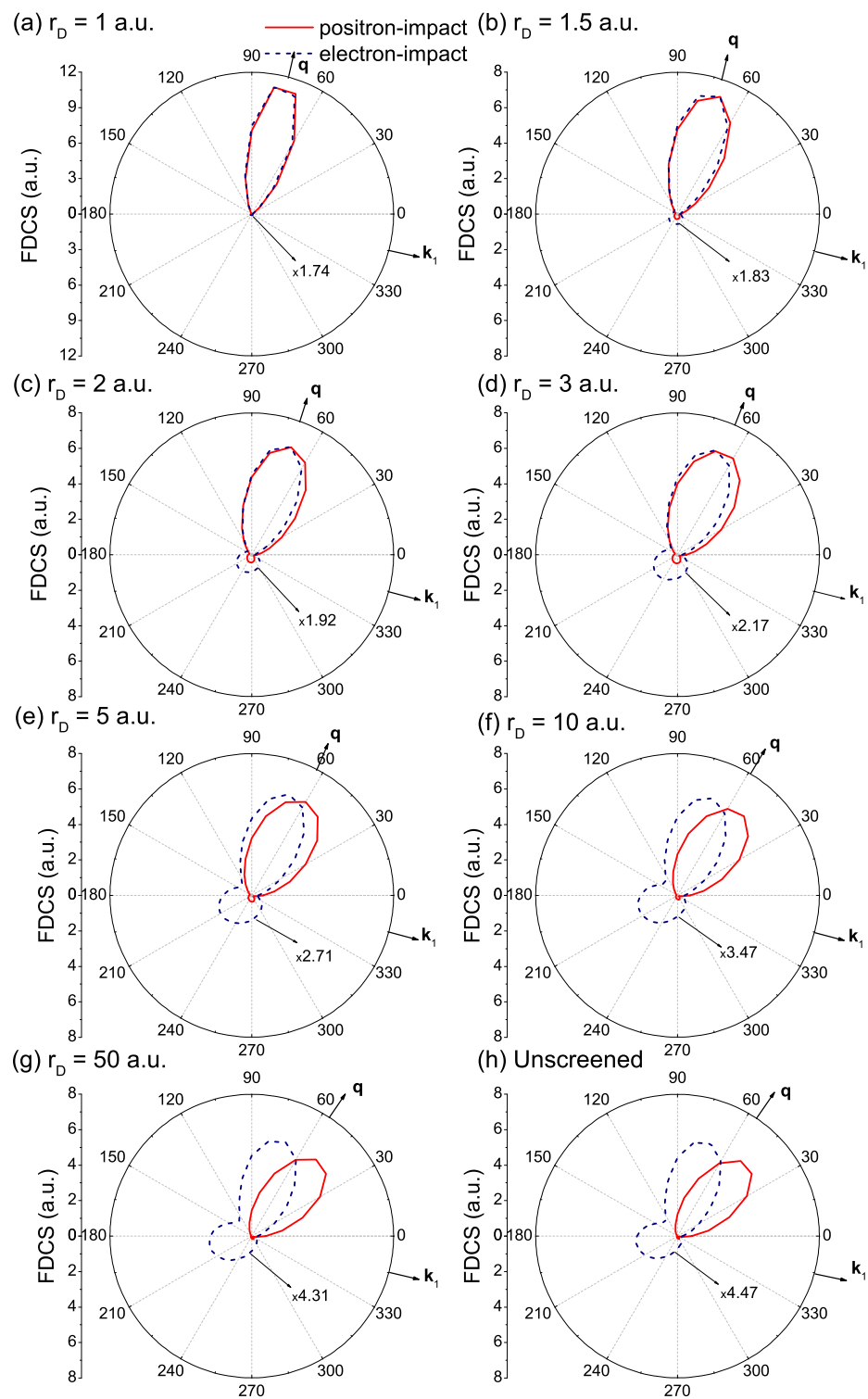


Figure 6. The same visualization as in Figure 4 but for $\theta_1 = -15^\circ$.

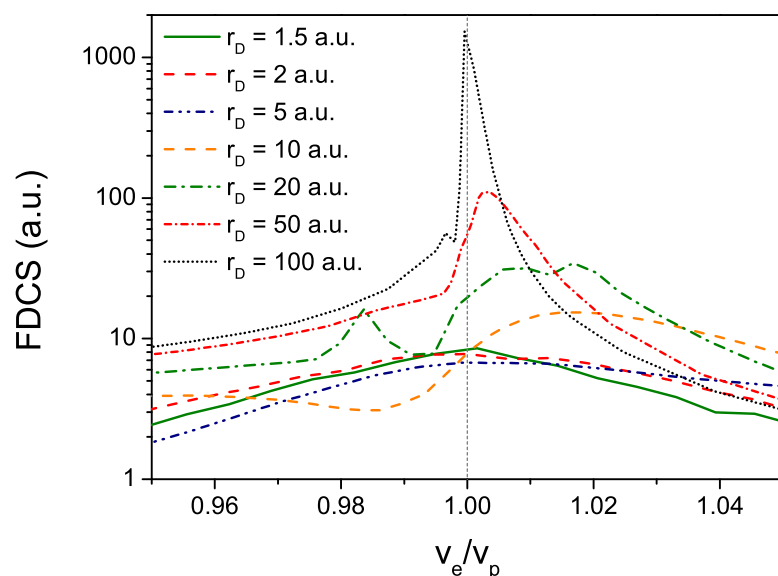


Figure 7. The Born-3DW fully differential cross section for forward emission in the scattering plane for the positron impact as a function of the ratio between the electron velocity and the projectile velocity v_e/v_p . The projectile scattering angle is set at 0° . The EEC peak position is indicated by a vertical dashed line. Cross sections are shown for different r_D -values.

Coming back to our case study, and since the Debye screening length affected the spatial window in which the particles conforming the system can interact with each other, the analysis of the ECC peak structure was expected to provide a complementary view on the decreasing role of the postcollisional interaction for decreasing r_D -values. Provided that the ionization potential of the hydrogen target diminished for decreasing r_D -values [18], we represented the FDCS in terms of the ratio between the electron velocity and the projectile velocity v_e/v_p . The ECC peak then corresponded to the case $v_e/v_p = 1$ (assuming both particles were emitted in the same direction). For $r_D = 100$ a.u., the asymmetric structure of the ECC peak was clearly predicted by the present theoretical model. Nonetheless, we noticed the presence of a small structure for electrons emitted with velocities slightly inferior to the projectile's. At present, we have not been able to determine the origin of that structure, which will be the object of future studies. As the screening increased, the structure of the peak dramatically changed. On the one hand, the magnitude of the structure was visibly affected. On the other hand, for r_D in the range 20 a.u.–10 a.u., the peak shifted to larger velocities from $v_e/v_p = 1$ showing a more complex structure. Only for $r_D < 5$ a.u. was a maximum recovered at that point but as a part of a much wider structure.

4. Conclusions

In this work, we performed a differential analysis of the positron impact ionization of hydrogen embedded in weak plasmas. In concordance with previous studies for positron and electron impact, the present CTMC results for the TCS indicated that the ionization became larger as the screening of the medium increased. In addition, our predictions for the SDCS in energy and angle suggested that as the screening increased, the postcollisional effects tended to lose relevance in the emitted electron spectrum. These statements were corroborated at the fully differential level by extending a Born-3DW model recently developed for screened environments that was previously tested in electron–hydrogen collisions. More studies are needed at this point in order to understand the sensitivity found for the ECC peak structure and its dynamics in terms of the Debye screening length.

Author Contributions: E.A. developed the Born-3DW code, performed numerical calculations, and contributed to the final manuscript. S.H.M. performed numerical Born-3DW numerical calculations and contributed to the final manuscript. S.O. performed CTMC calculations and supervised the project. All authors have read and agreed to the published version of the manuscript.

Funding: This work was supported by Grant No. PGI-24/F084, Secretaría General de Ciencia y Tecnología, Universidad Nacional del Sur.

Data Availability Statement: The data that support the findings of this study are available from the corresponding author upon reasonable request.

Conflicts of Interest: The authors declare no conflicts of interest.

References

1. Mergel, V.; Dörner, R.; Ullrich, J.; Jagutzki, O.; Lencinas, S.; Nüttgens, S.; Spielberger, L.; Unverzagt, M.; Cocke, C.L.; Olson, R.E.; et al. State Selective Scattering Angle Dependent Capture Cross Sections Measured by Cold Target Recoil Ion Momentum Spectroscopy. *Phys. Rev. Lett.* **1995**, *74*, 2200–2203. [[CrossRef](#)]
2. Ullrich, J.; Moshhammer, R.; Dorn, A.; Dörner, R.; Schmidt, L.; Schmidt-Böcking, H. Recoil-ion and electron momentum spectroscopy: Reaction-microscopes. *Rep. Prog. Phys.* **2003**, *66*, 1463–1545. [[CrossRef](#)]
3. Kövér, Á.M.; Laricchia, G. Triply Differential Study of Positron Impact Ionization of H₂. *Phys. Rev. Lett.* **1998**, *80*, 5309–5312. [[CrossRef](#)]
4. Armitage, S.; Leslie, D.E.; Garner, A.J.; Laricchia, G. Fragmentation of Positronium in Collision with He Atoms. *Phys. Rev. Lett.* **2002**, *89*, 173402. [[CrossRef](#)]
5. de Lucio, O.G.; Otranto, S.; Olson, R.E.; DuBois, R.D. Triply Differential Single Ionization of Argon: Charge Effects for Positron and Electron Impact. *Phys. Rev. Lett.* **2010**, *104*, 163201. [[CrossRef](#)]
6. Pflüger, T.; Holzwarth, M.; Senftleben, A.; Ren, X.; Dorn, A.; Ullrich, J.; Hargreaves, L.R.; Lohmann, B.; Slaughter, D.S.; Sullivan, J.P.; et al. Kinematically complete experiments for positron-impact ionization of helium atoms at the NEPOMUC facility. *J. Phys. Conf. Ser.* **2011**, *262*, 012047. [[CrossRef](#)]
7. DuBois, R.D.; de Lucio, O.G. Triply Differential Positron and Electron Impact Ionization of Argon: Systematic Features and Scaling. *Atoms* **2021**, *9*, 78. [[CrossRef](#)]
8. Arcidiacono, C.; Kövér, Á.; Laricchia, G. Energy-Sharing Asymmetries in Ionization by Positron Impact. *Phys. Rev. Lett.* **2005**, *95*, 223202. [[CrossRef](#)]
9. Fiol, J.; Barrachina, R.O. Continuum-orientation phenomena in ionization by positron impact. *J. Phys. B At. Mol. Opt. Phys.* **2011**, *44*, 075205. [[CrossRef](#)]
10. Zhang, S.B.; Qi, Y.Y.; Qu, Y.Z.; Chen, X.J.; Wang, J.G. Positron-impact excitation of hydrogen atoms in Debye plasmas. *Chin. Phys. Lett.* **2010**, *27*, 013401.
11. Nayek, S.; Ghoshal, A. ns → n's transition of hydrogen atom by positron impact with screened Coulomb interactions. *Eur. Phys. J. D* **2011**, *64*, 257–268. [[CrossRef](#)]
12. Rej, P.; Ghoshal, A. Positron impact excitations of hydrogen atom embedded in weakly coupled plasmas: Formation of Rydberg atoms. *Phys. Plasmas* **2014**, *21*, 093507. [[CrossRef](#)]
13. Rej, P.; Ghoshal, A. Positron impact excitations of hydrogen atom embedded in dense quantum plasmas: Formation of Rydberg atoms. *Phys. Plasmas* **2014**, *21*, 113509. [[CrossRef](#)]
14. Zammit, M.C.; Fursa, D.V.; Bray, I. Convergent-close-coupling calculations for excitation and ionization processes of electron-hydrogen collisions in Debye plasmas. *Phys. Rev. A* **2010**, *82*, 052705. [[CrossRef](#)]
15. Zammit, M.C.; Fursa, D.V.; Bray, I.; Janev, R.K. Electron-helium scattering in Debye plasmas. *Phys. Rev. A* **2011**, *84*, 052705. [[CrossRef](#)]
16. Sen, S.; Mandal, P.; Mukherjee, P.K. Positronium formation in Debye plasma. *Eur. Phys. J. D* **2011**, *62*, 379–388. [[CrossRef](#)]
17. Ma, J.; Cheng, Y.; Wang, Y.C.; Zhou, Y. Positronium formation in positron-hydrogen collisions with Debye potentials. *Phys. Plasmas* **2012**, *19*, 063303. [[CrossRef](#)]
18. Acebal, E.; Cuenca, A.; Martínez, S.; Otranto, S. Fully differential analysis of the electron impact ionization of hydrogen in Debye plasmas. *Phys. Plasmas* **2021**, *28*, 123510. [[CrossRef](#)]
19. Abrines, R.; Percival, I.C. A generalized correspondence principle and proton-hydrogen collisions. *Proc. Phys. Soc.* **1966**, *88*, 873–883. [[CrossRef](#)]
20. Olson, R.E.; Salop, A. Charge-transfer and impact-ionization cross sections for fully and partially stripped positive ions colliding with atomic hydrogen. *Phys. Rev. A* **1977**, *16*, 531–541. [[CrossRef](#)]
21. Reinhold, C.O.; Falcón, C.A. Classical ionization and charge-transfer cross sections for H⁺ + He and H⁺ + Li⁺ collisions with consideration of model interactions. *Phys. Rev. A* **1986**, *33*, 3859–3866. [[CrossRef](#)] [[PubMed](#)]
22. Salvat, F.; Fernández-Varea, J.M.; Williamson, W., Jr. Accurate numerical solution of the radial Schrödinger and Dirac wave equations. *Comput. Phys. Commun.* **1995**, *90*, 151–168. [[CrossRef](#)]

23. Brauner, M.; Briggs, J.S.; Klar, H. Triply-differential cross sections for ionisation of hydrogen atoms by electrons and positrons. *J. Phys. B At. Mol. Opt. Phys.* **1989**, *22*, 2265–2287. [[CrossRef](#)]
24. Garibotti, C.R.; Miraglia, J.E. Ionization and electron capture to the continuum in the H^+ -hydrogen-atom collision. *Phys. Rev. A* **1980**, *21*, 572–580. [[CrossRef](#)]
25. Hahn, T. CUBA—A library for multidimensional numerical integration. *Comput. Phys. Commun.* **2005**, *168*, 78–95. [[CrossRef](#)]
26. Malcherek, A.W.; Briggs, J.S. The n -electron Coulomb continuum. *J. Phys. B At. Mol. Opt. Phys.* **1997**, *30*, 4419–4433. [[CrossRef](#)]
27. Zhang, H.; Wang, J.G.; He, B.; Qiu, Y.B. Charge exchange and ionization in hydrogen atom-fully stripped ion collisions in Debye plasmas. *Phys. Plasmas* **2007**, *14*, 053505. [[CrossRef](#)]
28. Rogers, F.J.; Graboske, H.C., Jr.; Harwood, D.J. Bound Eigenstates of the Static Screened Coulomb Potential. *Phys. Rev. A* **1970**, *1*, 1577. [[CrossRef](#)]
29. Crooks, G.B.; Rudd, M.E. Experimental evidence for the mechanism of charge transfer into continuum states. *Phys. Rev. Lett.* **1970**, *25*, 1599–1601. [[CrossRef](#)]
30. Bernardi, G.C.; Suárez, S.; Fainstein, P.D.; Garibotti, C.R.; Meckbach, W.; Focke, P. Two-center effects in electron emission in $^3\text{He}^{2+}$ -He and H^+ -He collisions at intermediate energies. *Phys. Rev. A* **1989**, *40*, 6863–6872. [[CrossRef](#)]
31. Reinhold, C.O.; Olson, R.E. Classical two-center effects in ejected-electron spectra from p^+ , p^- and He^{2+} +He collisions at intermediate energies. *Phys. Rev. A* **1989**, *39*, 3861–3870. [[CrossRef](#)] [[PubMed](#)]
32. Fainstein, P.D.; Ponce, V.H.; Rivarola, R.D. Two-centre effects in ionization by ion impact. *J. Phys. B At. Mol. Opt. Phys.* **1991**, *24*, 3091–3119. [[CrossRef](#)]
33. Barrachina, R.O. Final-state interaction theory of cusp formation. *Nucl. Inst. Meth. Phys. Res. B* **1997**, *124*, 198–205. [[CrossRef](#)]
34. Brauner, M.; Briggs, J.S. Ionisation to the projectile continuum by positron and electron collisions with neutral atoms. *J. Phys. B At. Mol. Opt. Phys.* **1986**, *19*, L325–L330. [[CrossRef](#)]
35. Fiol, J.; Rodríguez, V.D.; Barrachina, R.O. Electron capture to the continuum by proton and positron impact. *J. Phys. B At. Mol. Opt. Phys.* **2001**, *34*, 933–944. [[CrossRef](#)]

Disclaimer/Publisher’s Note: The statements, opinions and data contained in all publications are solely those of the individual author(s) and contributor(s) and not of MDPI and/or the editor(s). MDPI and/or the editor(s) disclaim responsibility for any injury to people or property resulting from any ideas, methods, instructions or products referred to in the content.